LiDAR Measurements to Investigate Farm-to-Farm Interactions at the AWAKEN Experiment

Matteo Puccioni[1], Giacomo Valerio Iungo[1,*], Coleman Moss[1], Mojtaba Shams Solari[1], Stefano Letizia[2], Nicola Bodini[2], and Patrick Moriarty[2]

[1] Wind Fluids and Experiments (WindFluX) Laboratory, The University of Texas at Dallas, Richardson, TX, USA
[2] National Renewable Energy Laboratory (NREL), Golden, CO, USA

E-mail: valerio.iungo@utdallas.edu

Abstract. The exponential growth of wind energy and the need to exploit wind resources over areas with higher energy potential have led to the construction of neighboring wind turbines and farms with relatively small separation distances. As a result, for specific wind and atmospheric conditions, the wakes generated by an upstream wind farm may affect wind resources available for a downstream wind farm resulting in detrimental impacts on energy harvesting and structural loads for the downwind wind turbines. Distances between neighboring wind farms are typically larger than those associated with intra-wind-farm wake interactions, generating cumulative wakes whose characteristics might differ from those predicted through classical engineering wake models. These phenomena are referred to as farm-to-farm interactions. A better understanding and characterization of farm-to-farm interactions is one of the science goals tackled by the ongoing American WAKE experimeNt (AWAKEN). The site under investigation for this field campaign comprises two large wind farms in northern Oklahoma, USA, which are spaced roughly 5 km apart along the prevailing South-North wind direction. To investigate possible interactions between these two wind farms, the WindFluX mobile LiDAR station has been deployed mainly to perform volumetric scans over their gap region. In this paper, preliminary results from these LiDAR volumetric scans will be discussed, specifically for a case with multiple wind turbine wakes evolving during the occurrence of a low-level jet.

1. Introduction

As wind energy becomes one of the largest renewable energy sources in the United States [1], new challenges of modern wind power plants arise, such as the deployment of wind farms in complex terrain, design and control of turbine rotors able to generate more power even at low wind speeds, and the complex flow interactions occurring between closely-arranged wind turbines and farms [2–4]. To investigate these topics, the U.S. Department of Energy has funded the American WAKE experimeNt (AWAKEN) [5], which focuses on wind farms located in the Southern Great Plains in Oklahoma. A breadth of instruments has been deployed around five closely-spaced wind farms (King Plains, Armadillo Flats, Chisholm View, Breckinridge, and Thunder Ranch), and distributed over 13 ground-based sites and 4 wind turbines [6]. Among them, scanning pulsed Doppler wind light detection and ranging (LiDAR) represents a primary asset for the present study given its long scanning range (> 2000 m), its high temporal (≈ 1 s) and spatial resolution (≈ 20 m), and its flexible scanning strategies. Doppler wind LiDARs have

been successfully used to quantify both atmospheric-boundary-layer (ABL)-related events, such as low-level jets (LLJs) [7, 8], and wind farm-related phenomena, such as global blockage [9] and wake losses [3, 10]. Furthermore, the long range scanned by pulsed Doppler wind LiDARs makes this instrument compelling for investigation of farm-to-farm interactions, whose impact on annual energy production (AEP) still has not been fully quantified [11].

Preliminary analysis using supervisory control and data acquisition (SCADA) data available from the King Plains wind turbines has indicated the occurrence of velocity deficits for the first turbine row for Southerly winds [12]. Given the relatively short distance between the King Plains and Armadillo Flats wind plants along the North-South direction, this result can be interpreted as the effect of cumulative wakes originating from the Armadillo Flats wind farm. Thus, the use of scanning Doppler LiDARs will provide a three-dimensional view of the occurrence and extent of cumulative wakes reaching the King Plains wind plant.

In this work, preliminary results from the ongoing AWAKEN campaign are presented. The data have been collected with the WindFluX mobile LiDAR station of the University of Texas at Dallas (UTD) deployed between the King Plains and Armadillo Flats wind farms since October 2022. The analysis presented hereinafter will mainly focus on the characterization of multiple wind turbine wakes during the occurrence of LLJs. The remainder of this paper is organized as follows. In Section 2, the experimental site and the WindFluX mobile LiDAR station will be described. In Section 3, the scanning strategy adopted for the AWAKEN campaign will be detailed. In Section 4, the climatology of the site will be described based on the current availability of LiDAR data. In Section 5, an example of three-dimensional flow reconstruction involving wakes and LLJ will be illustrated. Finally, concluding remarks are reported in Section 6.

2. Experimental setup

The WindFluX mobile LiDAR station has been deployed at the AWAKEN site C1a (GPS: $36^\circ\,21'\,42.03''$N; $97^\circ\,30'\,35.95''$W, local time: UTC – 6h), which is located between the King Plains and Armadillo Flats wind farms, whose separation along the prevailing South-South-West wind direction is roughly 5 km. The main objective of the experimental setup is to capture both inlet and outlet flows of the wind farms. An overview of the experimental site is reported in Fig. 1. The WindFluX mobile LiDAR station encompasses one surface flux station and two scanning pulsed Doppler wind LiDARs, namely a Windcube 200S manufactured by Leosphere and a Streamline XR manufactured by Halo Photonics. The surface flux station is equipped with two CSAT3-3D sonic anemometers placed along the North-South direction, one WMS–302 cup-and-vane system, one PM–107 thermistor, and one HMP–155 temperature and relative humidity probe, all of them manufactured by Campbell Scientific except for the HMP–155 probe manufactured by Vaisala. A photo of the WindFluX mobile LiDAR station deployed at site C1a is reported in Fig. 1b.

In this work, a right-handed reference frame (x, y, z) oriented along streamwise, spanwise, and vertical directions, respectively, is used. The instantaneous wind vector is oriented accordingly, whose components are (u, v, w), while t is time. Prime indices refer to fluctuations in time and capital letters indicate time-averaged quantities.

The wind farm located North of the experimental station (King Plains) comprises 88 General Electric (GE) wind turbines featuring a diameter of $D = 127\,\mathrm{m}$, rated power of 2.82 MW, and hub-height of $H = 90\,\mathrm{m}$ [6, 13] (cyan symbols in Fig. 1a). The portion of the wind farm on South of the experimental station (Armadillo Flats) closer to site C1a consists of 2.3-MW GE wind turbines with a rotor diameter of $D = 116\,\mathrm{m}$ and hub-height of $H = 90\,\mathrm{m}$ (blue symbols in Fig. 1a) [6].

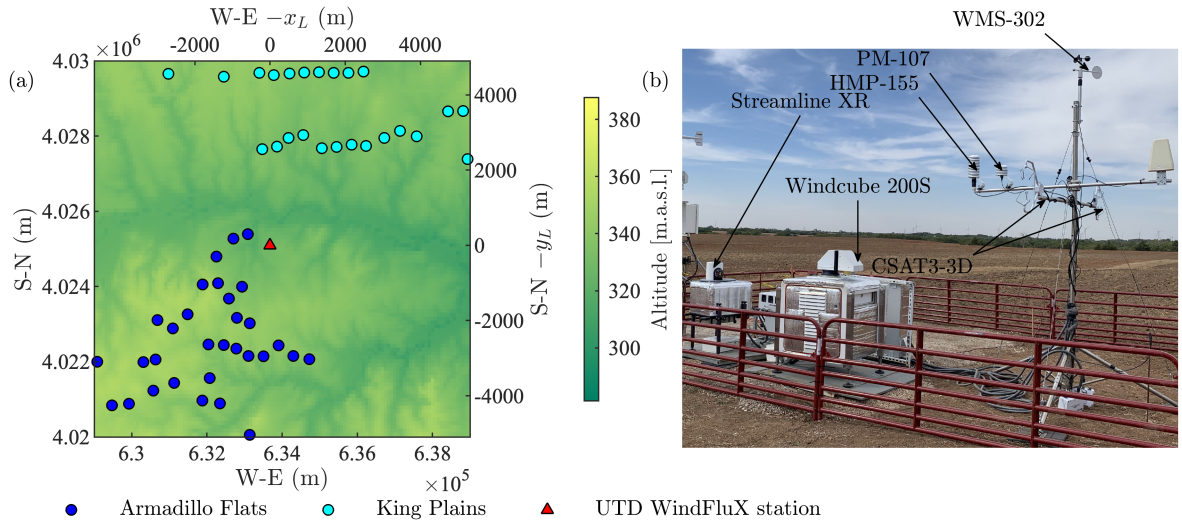

Figure 1. Overview of the experimental site. (a) Topography of the site C1a, terrain altitude, and turbine locations (information provided by the Atmospheric Radiation Measurement (ARM) database), both as GPS position and with respect to the LiDAR location (x_L, y_L); (b) WindFluX mobile LiDAR station.

Table 1. Summary of LiDAR scans designed for the AWAKEN campaign. T indicates the total scan duration, N_{rep} is the number of repetitions, τ is the sampling time, Θ ($\Delta\Theta$) is the azimuth angle (resolution) and Φ ($\Delta\Phi$) is the elevation angle (resolution). The acronym "VS" indicate volumetric scan.

LiDAR	Scan	T	N_{rep}	τ	Θ ($\Delta\Theta$)	Φ ($\Delta\Phi$)
XR	RHI	426 s	13	0.8 s 1.1 s 0.8 s	Feedback mode (0°)	0° − 10° (1°), 11° − 163° (4°), 167° − 180° (1°)
	DBS	623 s	25	3.8 s	[0, 72, 144, 216, 288, 0]°	[45, 45, 45, 45, 45, 0]°
	Stare	600 s	1200	0.5 s	N/A	90° (0°)
	VS	999 s	1	0.7 s	90° − 240° (1°)	[1, 2, 3, 4 − 28]° (2°)
200S	VS	1380 s	1	0.5 s	300° − 90° (1°)	[1, 1.5, 2, 3, 4 − 28]° (2°)

3. Optimal design and post-processing of LiDAR scans through LiSBOA algorithm

During the first months of the AWAKEN campaign, the scanning LiDARs performed a suite of different scans, which are summarized in Tab. 1; for the Streamline XR LiDAR, the total duration of the scan schedule is nearly 44 minutes. For the Streamline XR LiDAR, a DBS scan was designed to retrieve vertical profiles of time-averaged horizontal wind speed (V_h) and direction (Θ_w) under the assumption of horizontally-homogeneous flow. Specifically, five out of six beams are equally spaced between 0° and 360° with a 45° elevation angle, while the last beam is oriented vertically (cf. with Tab. 1) [14].

The Streamline XR LiDAR is further utilized to perform 0°–to–180° Range Height Indicator (RHI) scans to probe the streamwise wind speed, u, over the vertical plane aligned with the mean wind direction. The latter is measured at a height of 104 m with a dedicated DBS scan

performed before the RHI scans.

Another scan implemented for the Streamline XR LiDAR is a 10-minute-long vertical staring scan ($\Phi = 90°$). This scan is used to retrieve high-frequency (2 Hz) time series of the vertical wind component and backscatter coefficient, which can be used to describe several turbulence-related quantities, such as gravity waves, ABL height [15, 16], turbulent kinetic energy dissipation rate [15], vertical velocity variance, and mixed-layer height [17, 18].

The last scan, which is implemented for both LiDARs, is a volumetric scan aiming to reconstruct the spatial distribution of first- and second-order statistics of the streamwise velocity in the proximity of the wind farms. A volumetric scan consists of a sequence of Plane Position Indicator (PPI) scans with increasing elevation angle over a certain azimuth sector. Assuming a prevailing wind direction from SSE [13, 19], the Windcube 200S azimuth range is chosen to sample the flow around the King Plains wind farm, while the azimuth sector for the Streamline XR LiDAR is oriented towards the Armadillo Flats wind farm.

All the other volumetric-scan parameters are optimally selected based on the LiDAR Statistical Barnes Objective Analysis (LiSBOA) algorithm [20, 21]. The latter, assuming as input the instantaneous LiDAR velocity samples, is able to return the spatial distributions of time-averaged streamwise velocity statistics (mean, standard deviation, etc.) reconstructed over a user-defined Cartesian domain. However, due to the finite resolution associated with the LiDAR's gate length, the spatial variability of the velocity field can be reconstructed only down to a finite half-wavelength vector $\Delta\mathbf{n} = (\Delta n_x, \Delta n_y, \Delta n_z)$, which is selected by the LiDAR user. For a given half-wavelength vector, only a sub-portion of the chosen domain (closer to the LiDAR location) will respect the anti-aliasing constraint. The domain portion under-resolved by the chosen scanning configuration will then be minimized by volumetric scans featuring high azimuth/elevation resolutions $(\Delta\Theta, \Delta\Phi)$. However, any high spatial-resolution volumetric scan entails inevitably larger sampling periods and, thus, fewer scan repetitions for a given time. This selection can penalize the statistical uncertainty on the reconstructed mean velocity field, which would rather benefit from a low-resolution scan and a higher number of repetitions. Therefore, an optimally-designed volumetric scan is a trade-off between spatial and temporal resolutions [20].

For the AWAKEN campaign, an elevation range of $[1°, 28°]$ is chosen to have a thorough reconstruction of the streamwise wind speed. Assuming a Cartesian reference frame centered at the LiDAR location and oriented along the incoming wind direction, the streamwise extent of the Cartesian domain is set equal to $[100, 3000]$ m (assuming a maximum available range of 3000 m with high backscatter signal), while the spanwise range is assumed equal to $[-1500, 1500]$ m in order to reconstruct the mean flow around all the surrounding turbines. Finally, the vertical size of the Cartesian domain is chosen from $z \approx H - 0.65D$ (≈ 7 m) to $z \approx H + 5D$ (≈ 725 m).

To investigate wind turbine wakes, the reconstructed half-wavelengths are selected as multiples of the turbine diameters, D ($\Delta n_x = 3D$, $\Delta n_y = 0.5D$, $\Delta n_z = 0.5D$). Assuming four points to reconstruct a specific wavelength in each direction, the resolution of the reconstructed grid is then: $(\mathrm{d}x, \mathrm{d}y, \mathrm{d}z) = (0.75\,D, 0.125\,D, 0.125\,D)$. Based on these considerations, the chosen azimuth/elevation resolutions for both LiDARs are $\Delta\Theta = 1°$, $\Delta\Phi = 2°$ while the resulting elevation angles are reported in Tab. 1.

After collecting radial wind speed data from volumetric scans, the velocity records are injected into the dynamic filtering algorithm [22] to remove outliers from the instantaneous samples. In particular, for each space-time sample, this algorithm isolates all the records located in a neighboring spatio-temporal domain of $(x, y, z, t) = (100\,\mathrm{m}, 100\,\mathrm{m}, 10\,\mathrm{m}, 1800\,\mathrm{s})$ and generates a bi-variate normalized probability density function in the $(V_r - \mathrm{CNR})$ space (CNR is the Carrier-to-Noise Ratio). All the occurrences less than a certain threshold (0.1% for Windcube data, 0.5% for Streamline XR data) are marked as outliers, removed, and replaced through a bi-harmonic interpolation algorithm. The instantaneous values of quality-controlled radial wind speed are

utilized to estimate the streamwise velocity. In particular, for low elevation angles ($\Phi < 30°$) the streamwise wind speed is approximated by [2]:

$$u(r, \Theta, \Phi, t) = \frac{v_r(r, \Theta, \Phi, t)}{\cos(\Theta - \Theta_w)\cos\Phi}. \quad (1)$$

Only velocity samples showing $|\Theta - \Theta_w| \leq 45°$ will be retained for further analysis to avoid excessive contamination from cross-wind velocity components. For this analysis, the wind direction is estimated at each height via Vertical Azimuth Display (VAD) technique based on the radial wind speed data from each PPI scan.

4. Overview of the experimental data set

Focusing on the analysis of wind LiDAR data, the vertical profiles of mean horizontal wind speed (V_h) and wind direction (Θ_w) are used to obtain wind roses at different heights from the ground within the domain of interest (0 m to 800 m). For the period 2022-10-04 to 2023-01-20, 1316 mean profiles of wind speed and direction are available for this analysis. The result is reported in Fig. 2 for six heights between 85 m (hub height is 90 m) and 800 m. As inferred from Fig. 2, the prevalent wind direction is SSW throughout the scanned heights followed by a second peak (characterized by lower wind speed) located at NNE, consistent with previous climatology

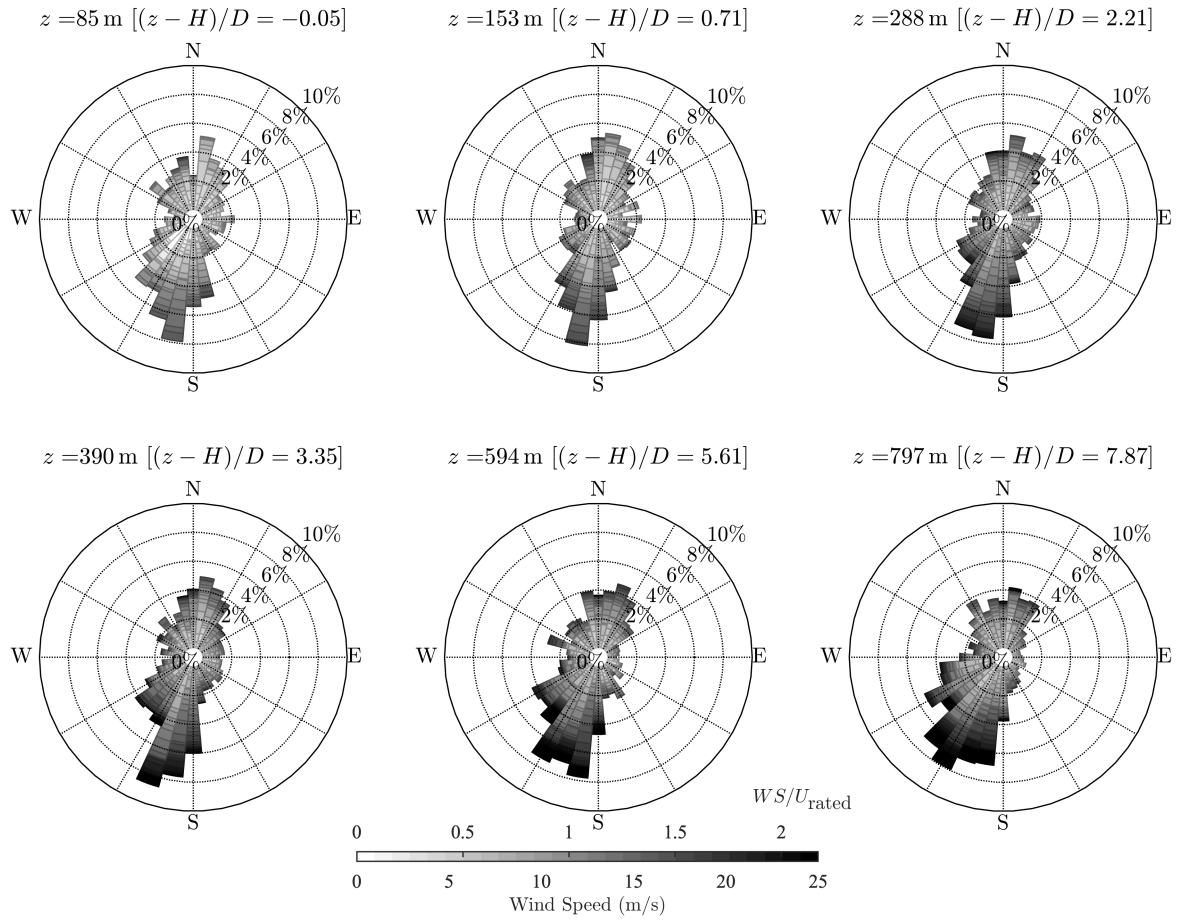

Figure 2. Wind roses retrieved from DBS mean velocity profiles at different heights from the ground, both dimensional and referred to the turbines rated wind speed (U_{rated}).

studies performed at the ARM facility located in the proximity of site C1a [13, 19]. However, from the wind rose at the height of 797 m, a significant clockwise shift towards SW is observed, which might be associated with the occurrence of veer [23].

Bi-hourly averaged profiles of wind speed and direction from DBS scans are calculated and reported in Fig. 3a–f for nighttime periods and in Fig. 3g–l for daytime periods. A subsequent best-fit is performed on each wind direction profile to extrapolate the hub-height value (Θ_h) and veer ($\Theta' = \mathrm{d}\Theta_w/\mathrm{d}z$ [24]) at different hours across the day:

$$\Theta_w(z) = \Theta_\mathrm{h} + \Theta'(z - z_H), \tag{2}$$

where z_H is the hub height. The calibrated values of Θ_h and Θ' are reported in Fig. 3 for each bin. High veer ($\Theta' = 0.05 - 0.07\,^\circ/\mathrm{m}$) is observed from 04:00 PM to 04:00 AM (local time) as opposed to the rest of the day ($\Theta' = 0.02 - 0.05\,^\circ/\mathrm{m}$), thus confirming the importance of veer and thermal stratification effects in determining the wind direction profile at different heights [23]. Wind shear is quantified by calibrating the shear exponent (α) over each bin-averaged

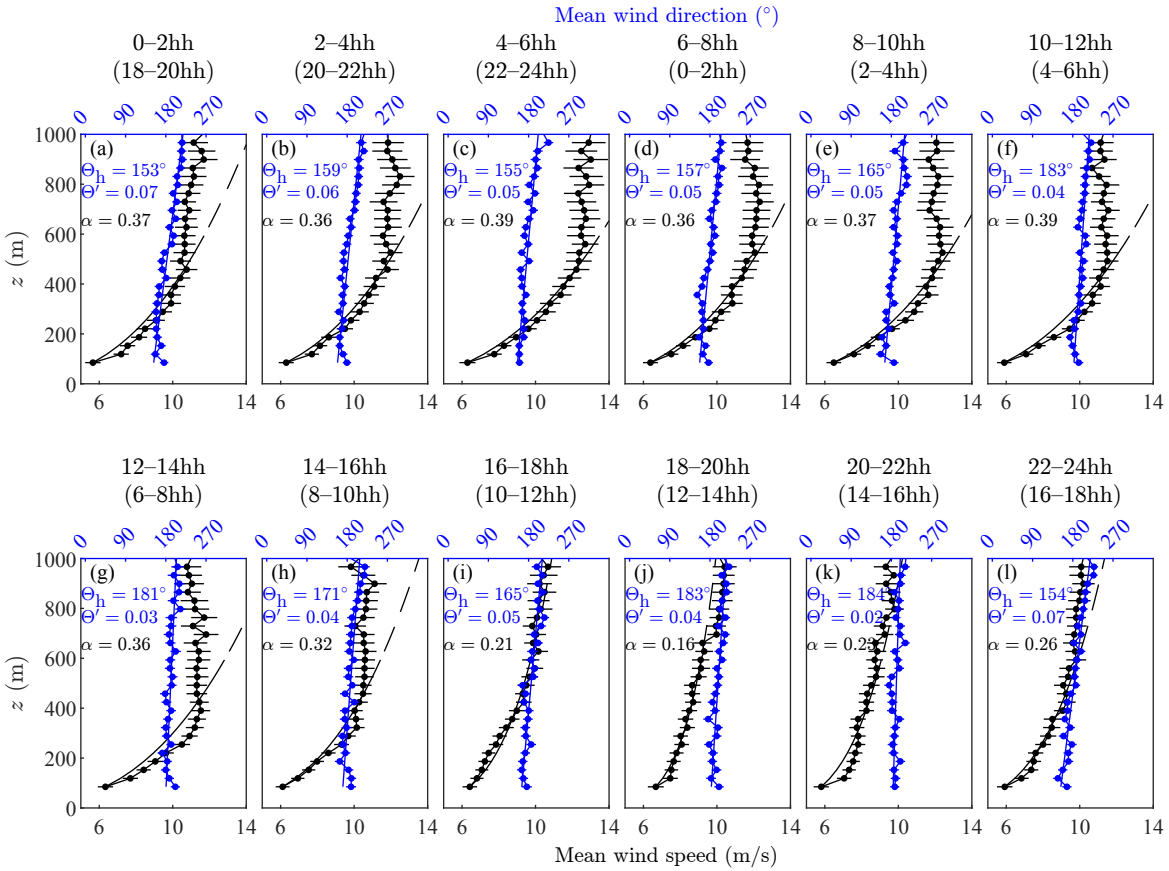

Figure 3. Vertical profiles of the mean horizontal wind speed (black symbols) and wind direction (blue symbols) reconstructed from DBS scans. (a–f): Nighttime. (g–l): Daytime. For each plot, the binning time is reported both in UTC and local time (in parenthesis). Θ_h and Θ' refer to the wind direction at hub height and veer, respectively. The dashed line reports the fitted wind speed profile above 600 m.

mean velocity profile according to the following equation [3, 25]:

$$\frac{U}{U_R} = \left(\frac{z}{z_R}\right)^{\alpha}, \tag{3}$$

where U_R and z_R represent the reference wind speed and height assumed at the lowest available gate ($z = 85\,\mathrm{m}$). Notably, α is tuned over heights up to $z = 600\,\mathrm{m}$, which represents the lowest ABL height previously measured throughout the day at the same site [19]. The calibrated values of the shear exponent for nighttime hours (06:00 PM to 06:00 AM) lie in the interval $0.37 \leq \alpha \leq 0.39$, as opposed to daytime shear exponents quantified between 0.16 and 0.36 (as reported in Fig. 3a–f and g–l, respectively). Thus, from mean profiles of wind speed and direction obtained through DBS scans, the effect of thermal stratification is inferred and translated into larger (smaller) shear and veer during nighttime (daytime).

5. LiDAR Data of Turbine Wakes Under the Occurrence of Low-Level Jet

The occurrence of LLJs at site C1a and their interactions with wind turbine wakes are investigated through the synergistic analysis of LiDAR volumetric scans (performed by both LiDARs) and DBS scans (performed only by the Streamline XR LiDAR). For the selected data collected on 2022-11-22 from 03:30 AM to 09:22 AM UTC, the vertical profiles of wind speed and direction obtained from the DBS scans evidence the occurrence of a consistent LLJ with a maximum velocity of $\approx 14\,\mathrm{m/s}$ located around 300-m height (Fig. 4) for the entire duration of the selected period. Furthermore, the wind direction profiles show low-veer conditions ($\Theta' \leq 0.04°/\mathrm{m}$) and roughly constant hub-height wind direction from SSE ($205° \leq \Theta_\mathrm{h} \leq 218°$).

The steadiness of the wind conditions for the selected period is also qualitatively cross-checked through the mean (Fig. 5a) and standard deviation (Fig. 5b) of the radial wind speed retrieved by the PPI scans performed with 3°–elevation angle from both LiDARs. Consistent wakes generated from the Armadillo Flats wind plant are identified both through velocity deficit and wake-generated turbulence intensity.

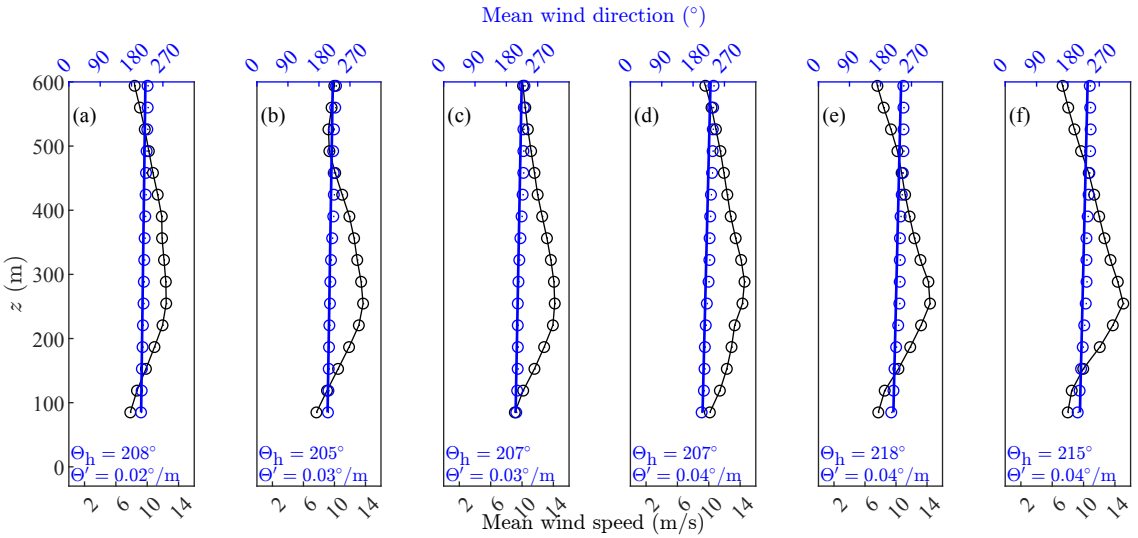

Figure 4. Vertical profiles of mean velocity and wind direction reconstructed from DBS scans on 2022-11-22 at different UTC times. (a) 03:30; (b) 04:40; (c) 05:51; (d) 07:01; (e) 08:12; (f) 09:22. Circle and cross symbols represent best-fitted values with R-square greater or lower than 0.90, respectively. Continuous blue line is the best fit with Eq. (2).

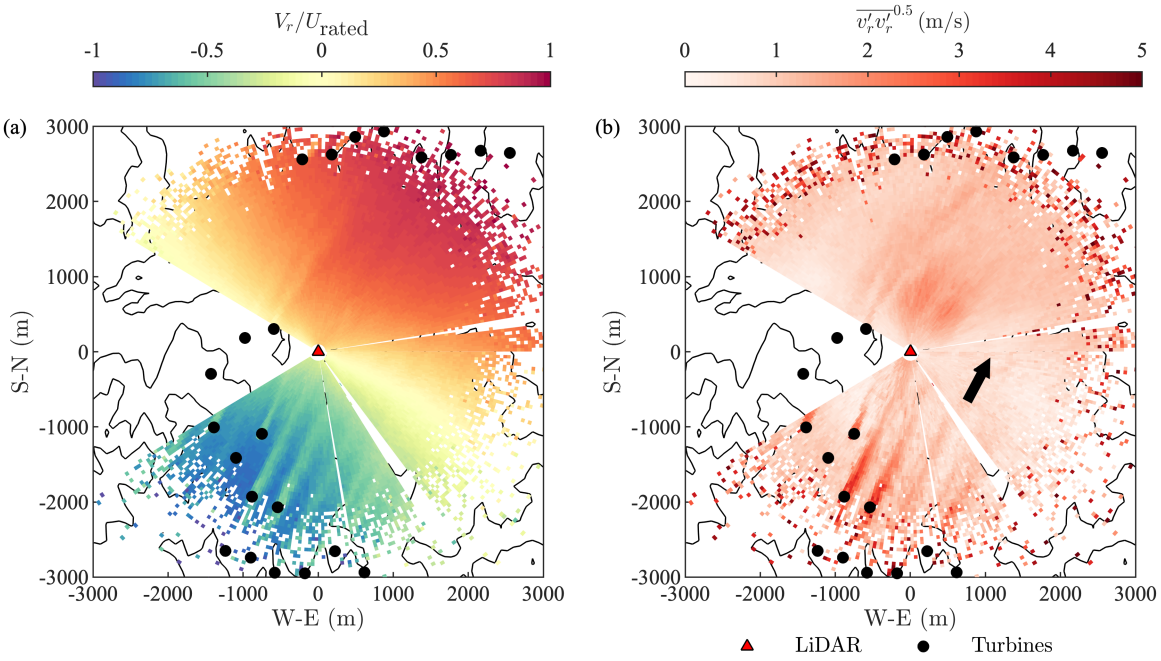

Figure 5. Radial wind speed made non-dimensional with the turbine rated wind speed (V_r/U_{rated}) sampled by the scanning Doppler LiDARs through PPI scans with 3° elevation angle over the entire period selected: (a) time average; (b) standard deviation (black arrow reports the mean hub-height wind direction measured by DBS scans).

The spatial flow variability is reconstructed through the LiSBOA algorithm applied to streamwise velocity collected by both LiDARs with volumetric scans. According to the scanning strategy designed via the LiSBOA algorithm, 5 volumetric scans are completed by the Streamline XR scanning LiDAR between 03:30 AM and 09:22 AM, while 17 volumetric scans are executed by the Windcube 200S LiDAR during the same period. For each PPI scan, the quality-controlled radial wind speed is used to estimate the streamwise wind speed via Eq. (1). Notably, the wind direction (Θ_w) used in Eq. (1) is reconstructed as a function of height for each volumetric scan through the velocity azimuth display (VAD) technique. Furthermore, the streamwise velocity is made non-dimensional with a reference ABL wind profile obtained at each height as 70^{th} percentile value from the entire volumetric-scan data [2]. Subsequently, non-dimensional streamwise mean wind speed and turbulence intensity (TI) are retrieved via the LiSBOA algorithm.

The result of this analysis is reported as horizontal sections in Fig. 6 for heights between $(z-H)/D = -0.25$ (≈ 57 m) and $(z-H)/D = 0.25$ (≈ 121 m) considering $D = 127$ m and $H = 89$ m for the King Plains turbines [13]. A median hub-height wind direction of $\Theta_{\text{h}} = 208°$ is used to rotate the local reference frame into global coordinates. From Fig. 6a–c, multiple wakes are detected over the South-East portion of the measurement domain. Further, a cumulative wake originating from the Armadillo Flats turbines on the North-West corner is observed to reach the first row of the King Plains wind plant; this phenomenon, already highlighted by previous studies on SCADA data for the same wind direction [12], evidences the occurrence of farm-to-farm interactions for the observed wind condition. An extensive study of this phenomenon will be possible upon the availability of more volumetric-scan data collected under different atmospheric and turbine operative conditions. The TI distribution reported in Fig. 6d–f shows high-TI wake patterns ($TI \geq 20\%$) over rotor heights, which can be associated with the downstream evolution

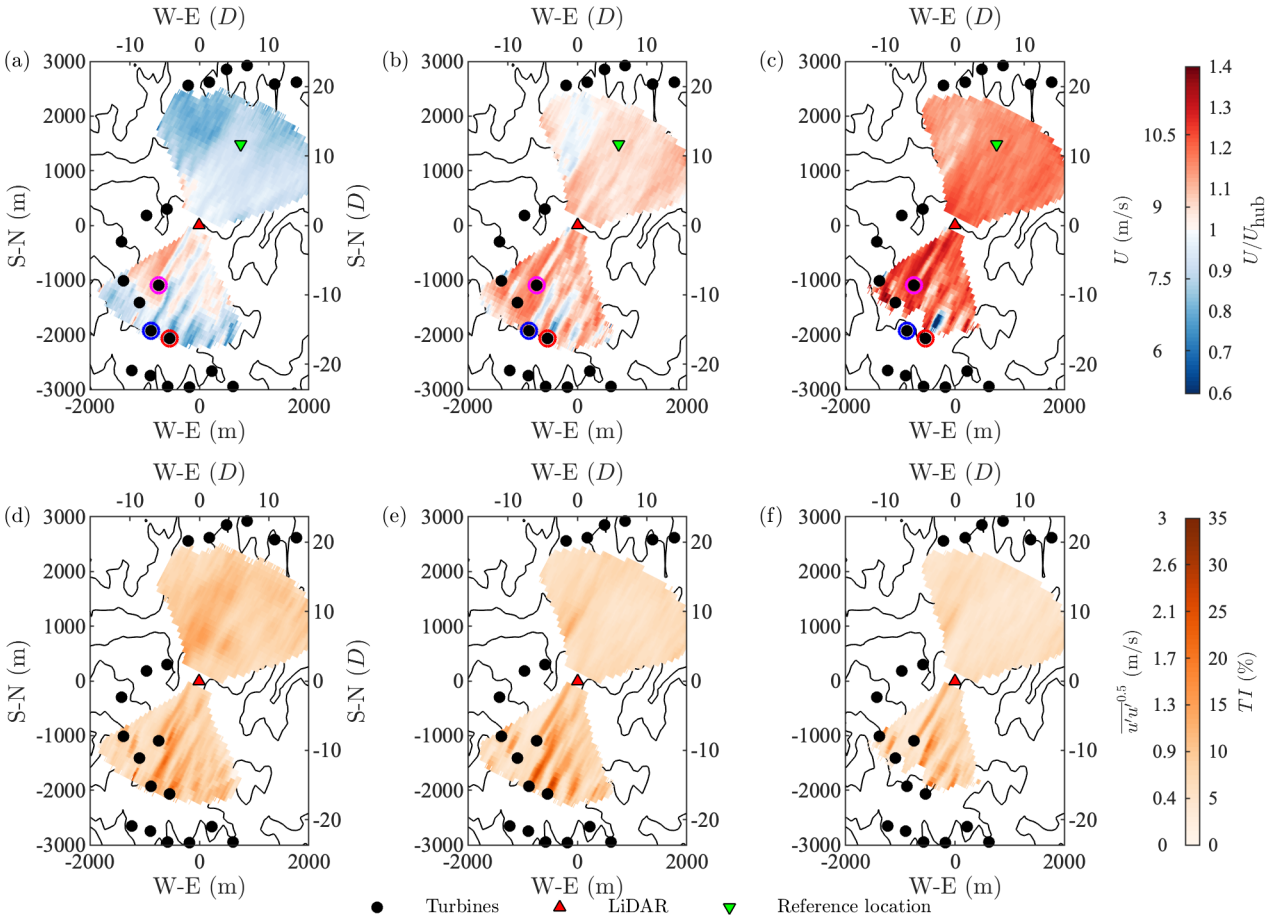

Figure 6. Mean streamwise velocity (a–c) and TI (d–f) evaluated at different heights from the ground: (a, d) $(z - H)/D = -0.25$; (b, e) 0; (c, f) 0.25.

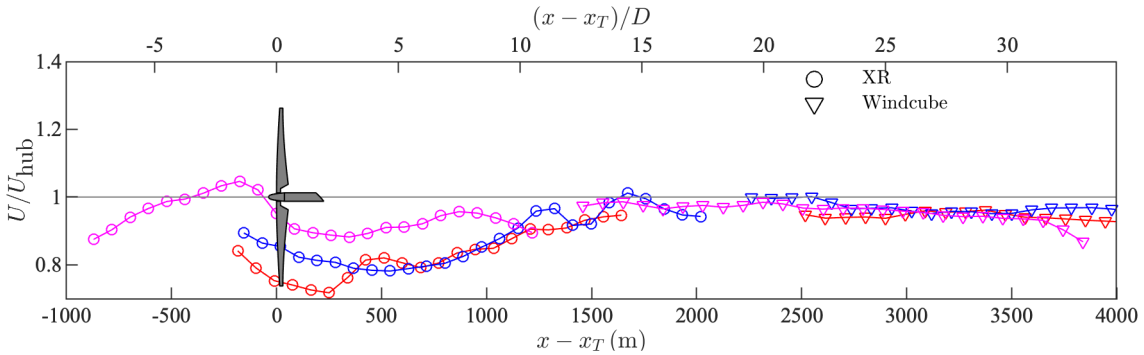

Figure 7. Hub-height mean wind speed as a function of the streamwise position; each color corresponds to a different turbine as reported in Fig. 6b.

of the wakes while low TI (less than 10%) is quantified outside of the wake regions.

The wakes generated by three turbines of the Armadillo Flats wind farm, which are reported in Fig. 6a–c with red, green, and blue circles, are further investigated in Fig. 7 considering

the mean velocity measured at hub height along the streamwise direction. It is observed that as $(x - x_T) \geq 20\,D$ (where x_T is the turbine's streamwise position) all the profiles generally recovers to the hub-height wind speed measured at the wind turbine location, meaning that the wakes generated from Armadillo Flats are practically completely recovered. For the streamwise positions reported in Fig. 7, the velocity deficit in the proximity of the rotor is quantified between nearly 0.7-0.9 U_∞ followed by an increase up to roughly $10\,D$ downstream where $U \approx U_{\text{hub}}$ ($U_{\text{hub}} = 8.5$ m/s for this data set), in agreement with previous LiDAR measurements of onshore wind farms [3].

It is interesting to examine the vertical profiles extracted from the volumetric scans at different locations along the center line of the selected wakes to characterize their downstream evolution. From the analysis of the mean wind speed profiles in Fig. 8a–d, very good agreement is found outside of the rotor area between the LiSBOA- and DBS-reconstructed mean velocity (black circle symbols), as well as between the profiles close to the turbines (red and green lines) and the reference undisturbed profile (black line), thus indicating low streamwise variability of LLJ.

As expected, velocity deficits are probed within the rotor area indicating the presence of wakes. The TI profiles within the rotor area (Fig. 8e–h) reveals wake-generated turbulence decreasing from $TI \approx 20\%$ to $TI \approx 10\%$ within $4.5\,D \leq (x - x_T) \leq 10.5\,D$, yet sensibly higher than the reference TI profile (black line) which shows a monotonically decreasing trend moving upward; by contrast, all the profiles collapse onto low TI values above the rotor area ($TI \leq 5\%$) following classic decaying distributions occurring for ABL flows [8].

The mean velocity deficit and wake-added TI with respect to the chosen reference profile (whose location is reported by the green triangular symbol in Fig. 7a–c) are reported in Fig. 9 for the above-mentioned streamwise/spanwise locations. In particular, for the streamwise positions relatively close to the turbines ($(x - x_T)/D = 4.5$) reported in Fig. 9a, a non-dimensional velocity deficit of $(U - U_{\text{hub}})/U_{\text{hub}} = -0.2$ is observed within the rotor area, which reduces to $(U - U_{\text{hub}})/U_{\text{hub}} \approx -0.15$ at $(x - x_T) = 6.5\,D$. Overall, the evolution of wind turbine wakes in presence of LLJ is identified. Similarly, the vertical distribution of wake-added TI (Fig. 9e)

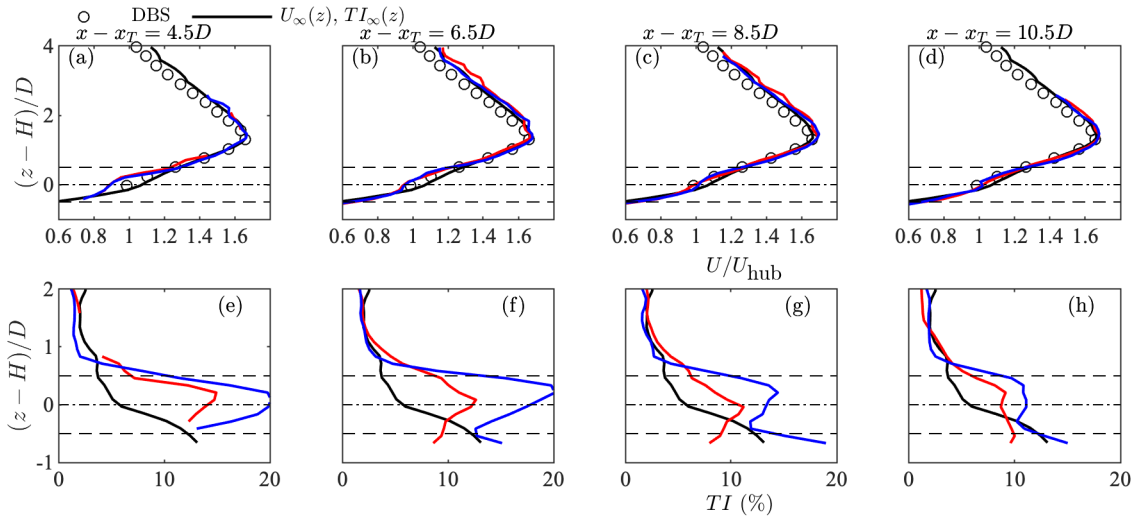

Figure 8. Vertical profiles of mean velocity (a–d) and TI (e–h) over different streamwise locations downstream to the wind turbine rotors along the turbine axes. Different colors correspond to profiles related to different turbines according to the color of circle symbols reported in Fig. 6. Black circle symbols represent the DBS wind profile, while the black lines are the reference wind speed and TI profiles reconstructed from the volumetric scans.

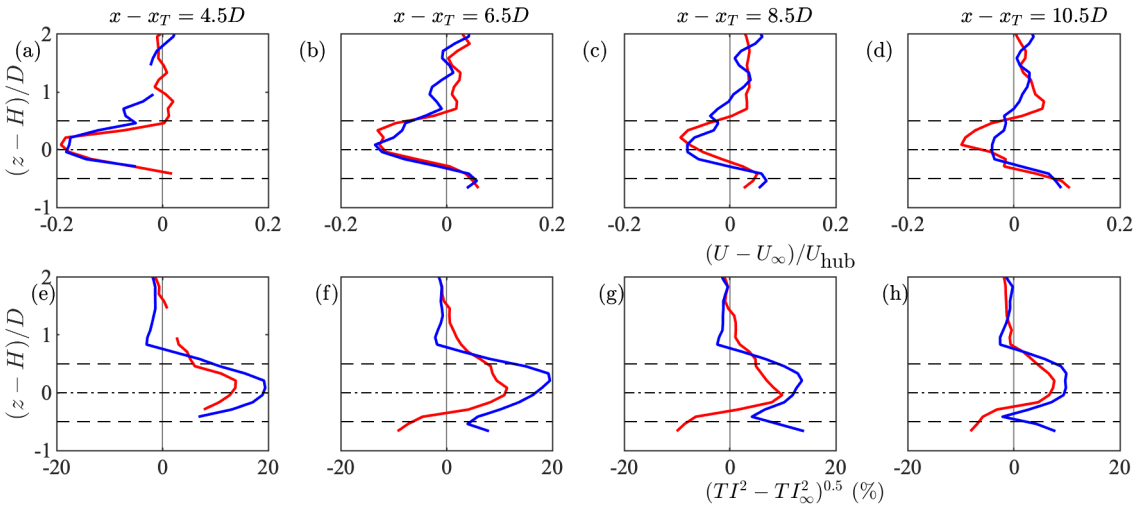

Figure 9. Vertical profiles of mean velocity deficit (a–d) and wake-added TI (e–h) for different streamwise locations downstream to the wind turbine rotors. Different colors correspond to different turbines, as reported in Fig. 6.

indicates a significant TI generation in the wake at $(x - x_T) = 4.5\,D$ (+20%) within the wake region.

6. Concluding remarks

In this study, preliminary results from the ongoing AWAKEN campaign have been presented. The experimental data have been collected starting from early October 2022 at the C1a site between the Armadillo Flats and King Plains wind farms near Enid, OK, with the WindFluX mobile LiDAR station, which comprises two ground-based pulsed Doppler wind LiDARs and one surface flux station.

A 6-hour-long period of volumetric LiDAR scans has been down-selected to investigate the evolution of multiple wind turbine wakes during the occurrence of a low-level jet (LLJ). The analysis of the LiDAR data has revealed a wake velocity deficit of 20% compared to the incoming wind speed within the rotor area at a downstream distance of 4.5 rotor diameters, which reduces to less than 10% after 10.5 rotor-diameter downstream. The analysis of the wake-added TI has revealed values of about 20% within the rotor area at $4.5\,D$ downstream of the rotor, which persists further downstream (10.5 D) where the intensity is about 10%.

Acknowledgments

This work was authored in part by the National Renewable Energy Laboratory, operated by Alliance for Sustainable Energy, LLC, for the U.S. Department of Energy (DOE) under Contract No. DE-AC36-08GO28308. Funding provided by the U.S. Department of Energy Office of Energy Efficiency and Renewable Energy Wind Energy Technologies Office. The views expressed in the article do not necessarily represent the views of the DOE or the U.S. Government. The U.S. Government retains and the publisher, by accepting the article for publication, acknowledges that the U.S. Government retains a nonexclusive, paid-up, irrevocable, worldwide license to publish or reproduce the published form of this work, or allow others to do so, for U.S. Government purposes.

References

[1] Wiser R, Bolinger M, Hoen B, Millstein D, Rand J, Barbose G, Darghouth N, Gorman W, Jeong S and Paulos B 2022 Land-based wind market report: 2022 edition Tech. rep. Lawrence Berkeley National Lab.(LBNL), Berkeley, CA (United States)
[2] Zhan L, Letizia S and Valerio Iungo G 2020 *Wind Energy* **23** 501–527
[3] El-Asha S, Zhan L and Iungo G V 2017 *Wind Energy* **20** 1823–1839
[4] Santhanagopalan V, Rotea M and Iungo G 2018 *Renewable Energy* **116** 232–243
[5] Moriarty P, Hamilton N, Debnath M, Herges T, Isom B, Lundquist J K, Maniaci D, Naughton B, Pauly R, Roadman J *et al.* 2020 American WAKe ExperimeNt (AWAKEN) Tech. rep. Lawrence Livermore National Lab.(LLNL), Livermore, CA (United States ...
[6] Moriarty P, Bodini N, Brugger P, Goldberger L, Herges T, Hirth B, Iungo G V, Ivanov H, Kaul C, Klein P, Krishnamurthy R, Letizia S, Lundquist K, Morris V R, Newsom R, Pekour M, Scholbrock A, Schroeder J, Simley E, Wharton S and Zalkind D 2023 *Journal of Renewable and Sustainable Energy* 1–42
[7] Banta R M, Newsom R K, Lundquist J K and Pichugina Y L 2002 *Boundary-Layer Meteorology* **105** 221–252
[8] Banta R M, Pichugina Y L and Brewer W A 2006 *Journal of the Atmospheric Sciences* **63** 2700–2719 ISSN 00224928
[9] Schneemann J, Theuer F, Rott A, Dörenkämper M and Kühn M 2021 *Wind Energy Science* **6 (2)** 521–538 ISSN 23667451
[10] Machefaux E, Larsen G C, Troldborg N, Hansen K S, Angelou N, Mikkelsen T and Mann J 2016 *Wind Energy* **19** 1535–1551
[11] Clifton A, Smith A and Fields M 2016 Wind plant preconstruction energy estimates. current practice and opportunities Tech. rep. National Renewable Energy Lab.(NREL), Golden, CO (United States)
[12] Moss C, Romit M, Patrick M and Iungo G V 2023 *Wind Energy*
[13] Debnath M, Scholbrock A K, Zalkind D, Moriarty P, Simley E, Hamilton N, Ivanov C, Arthur R S, Barthelmie R, Bodini N, Brewer A, Goldberger L, Herges T, Hirth B, Valerio Iungo G, Jager D, Kaul C, Klein P, Krishnamurthy R, Letizia S, Lundquist J K, Maniaci D, Newsom R, Pekour M, Pryor S C, Ritsche M T, Roadman J, Schroeder J, Shaw W J, Van Dam J and Wharton S 2022 *Journal of Physics: Conference Series* **2265** ISSN 17426596
[14] Sathe A, Mann J, Vasiljevic N and Lea G 2015 *Atmospheric Measurement Techniques* **8** 729–740 ISSN 18678548
[15] Kristensen L, Lenschow D, Kirkegaard P and Courtney M 1989 *Boundary Layer Studies and Applications* (Springer) pp 149–193
[16] Frehlich R, Hannon S M and Henderson S W 1998 *Boundary-Layer Meteorology* **86** 233–256 ISSN 00068314
[17] Steyn D G, Baldi M and Hoff R M 1999 *Journal of Atmospheric and Oceanic Technology* **16** 953–959 ISSN 07390572
[18] Stull R B 1988 *An introduction to boundary layer meteorology* vol 13 (Springer Science & Business Media)
[19] Krishnamurthy R, Newsom R K, Chand D and Shaw W J 2021 Boundary layer climatology at arm southern great plains Tech. rep. Pacific Northwest National Lab.(PNNL), Richland, WA (United States)
[20] Letizia S, Zhan L and Iungo G V 2021 *Atmospheric Measurement Techniques* **14** 2065–2093
[21] Letizia S, Zhan L and Iungo G V 2021 *Atmospheric Measurement Techniques* **14** 2095–2113
[22] Beck H and Kühn M 2017 *Remote Sensing* **9** ISSN 20724292
[23] van de Wiel B J, Moene A F, Steeneveld G J, Baas P, Bosveld F C and Holtslag A A 2010 *Journal of the Atmospheric Sciences* **67** 2679–2689 ISSN 00224928
[24] Kelly M and Laan M P V D 2023 *Wind Energy Discussion* 1–37
[25] Iungo G V and Porté-Agel F 2014 *Journal of Atmospheric and Oceanic Technology* **31** 2035–2048